Supplementary Information section including all the figures

Table 1. Specific parameters used on the different growths orientations (a:[11$\bar{2}$0], m:[10$\bar{1}$0], c:[0001])

Seed orientation	Number of windows in the after heater	Pulling rate [µm.min^{-1}]
a	1	500
a	3	500
m	1	500
m	3	500
c+30°	1	500
c+30°	3	500
c	1	500
c	3	500
a	1	50,100,200,400,600, 1200
a	3	50,100,200,400,600, 1200
m	1	50,100,200,400,600, 1200
m	3	50,100,200,400,600, 1200

Figures for supplementary information

Fig.S1. Sketch of a typical mirror suspension similar to that of KAGRA. a) substrate; b) coatings; c) fibers; d) nail heads welded on fibers; e) hears bonded on substrate;22 f) cantilever springs.

Fig. S2.(a) Thermal insulation configuration around the crucible, (b) Crucible, (c) After heater (one window (1GT)), (d) After heater (three window (3GT)).

Fig.3. The different sapphire growth steps by µ-PD technique.

Fig.4. Video images of bubble incorporation in sapphire rod grown by micro-pulling down technique.

Fig.5. Undoped sapphire rods grown by micro-pulling down technique.

Fig.S6. Wafers of sapphire. (a) sapphire grown by Czochralski technique using a[11$\bar{2}$0] axis seed orientations,(b) sapphire grown by Czochralski technique using r[10$\bar{1}$2] axis seed orientations and (c) crystals grown by Verneuil flame fusion technique.

F**ig.S7.** Bubbles densities variation along the rods (longitudinal), (a) a-axis; (b) m-axis; (c) c-axis and (d) the c-axis tilted of 30°. (Black squares: rods grown with the standard configuration of thermal gradient (After heater with one window (1GT)). red dots: rods grown with the configuration inducing high thermal gradient (after heater with three windows (3GT))). For all samples pulling rate was 500 µm.min-1.

Fig.S8. Rods cross section bubbles densities measured in different parts of sapphire crystals grown along different seed orientations: (a) a-axis; (b) m-axis; (c) c-axis and (d) c tilted of 30°. The measurements on the rods grown with a standard configuration of thermal gradient around the capillary are presented by black squares. The bubbles densities measured on the rods grown with the configuration inducing high thermal gradient are presented by red dots. For all samples pulling rate was 500µm.min-1.

Fig.9. Bubbles density variations as a function of the pulling rates. Observation on the lateral periphery of the grown rod in (a) V = 500 µm.min^{-1}; (b) V =1200 µm.min^{-1}. Observation on the cross section of the grown rod; (c) V = 500µm.min^{-1}; d) V=1200 µm.min^{-1}

Fig.S10. Bubbles arrangement in one array at about 100µm from the periphery of the rods (a) a-axis, v=1200µm.min-1, 1GT=40°C/mm, (b) a-axis, v=1200µm.min-1 , GT=55°C/mm, (c) m-axis, v=1200 µm.min-1 , GT=40°C/mm, (d) c+30°-axis, v=1200µm.min-1, GT=55°C/mm, (e) c-axis, v= 500µm.min-1, 1GT=40°C/mm.

Fig.S11. (a) Bubbles densities evolution on the barrel, (b)bubbles densities evolution on the cross section. (Squares = a-axis; triangles = m-axis; red = standard thermal gradient; black = high thermal gradient).

Fig.S12. Peak positions of the A1g mode around 417 cm-1 as a function of the position in the rod. (a) a-axis; (b) m-axis; (c) c-axis and (d) the c tilted of 30°. In black, measurements realized on a rods grown with the standard configuration of thermal gradient (1GT). In red, measurements realized on a rods grown with the configuration inducing high thermal gradient (3GT).

Fig.S13. Peak positions of the A1g mode around 417 cm-1 in function of the seed orientations, (a) in the beginning; (b) in the middle, and (c) in the end of the rod. In black, measurements realized on a rods grown with the standard configuration of thermal gradient (1GT). In red, measurements realized on a rods grown with the configuration inducing high thermal gradient (3GT).

Fig.14. Peak positions of the A1g mode around 417 cm^{-1} in function of the grown techniques and seed orientations.

Fig.15. LIBS measurements performed on (a) a bubble just below the surface and a second one deeper, in (b) a single bubble below the surface and in (c) region of sapphire rod without bubbles. Spectra intensities of different impurities are present in function of the laser shots number.

Fig.S16. Schematic illustration of bubbles distribution as a function of pulling rate, seed orientation and thermal gradient (1GT: standard thermal configuration, 3GT: high thermal gradient configuration). The crystallographic orientations are indicated by arrows.

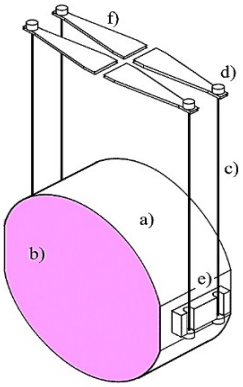

Fig.S1. Sketch of a typical mirror suspension similar to that of KAGRA. a) substrate; b) coatings; c) fibers; d) nail heads welded on fibers; e) hears bonded on substrate;[22] f) cantilever springs.

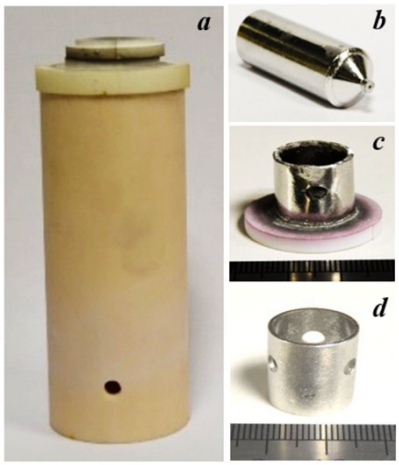

Fig.S2.(a) Thermal insulation configuration around the crucible, (b) Crucible, (c) After heater (one window (1GT)), (d) After heater (three window (3GT)).

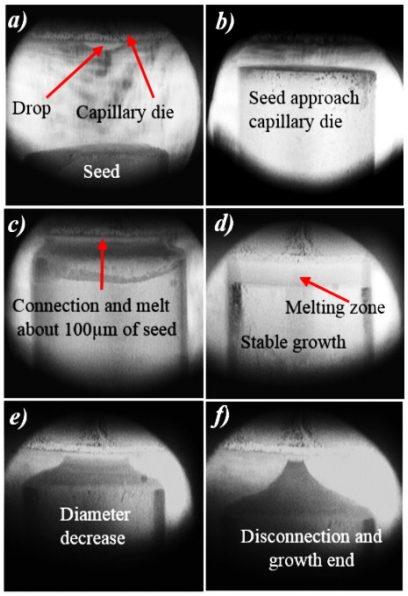

Figure 3. The different sapphire growth steps by µ-PD technique.

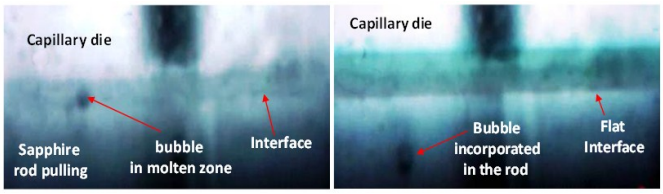

Figure 4. Video images of bubble incorporation in sapphire rod grown by micro-pulling down technique.

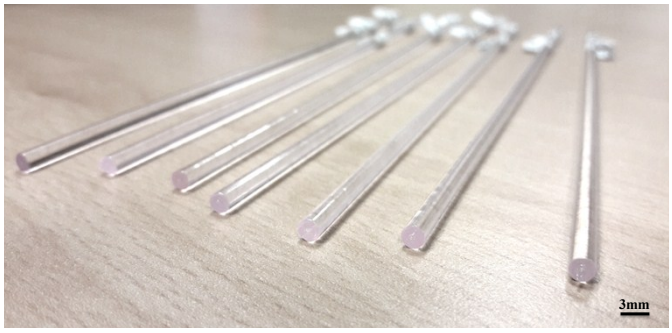

Figure 5. Undoped sapphire rods grown by micro-pulling down technique.

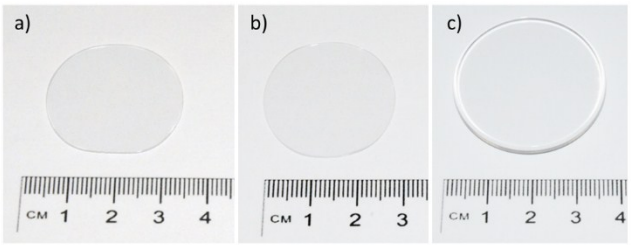

Fig.S6. Wafers of sapphire. (a) sapphire grown by Czochralski technique using a[11$\bar{2}$0] axis seed orientations,(b) sapphire grown by Czochralski technique using r[10$\bar{1}$2] axis seed orientations and (c) crystals grown by Verneuil flame fusion technique.

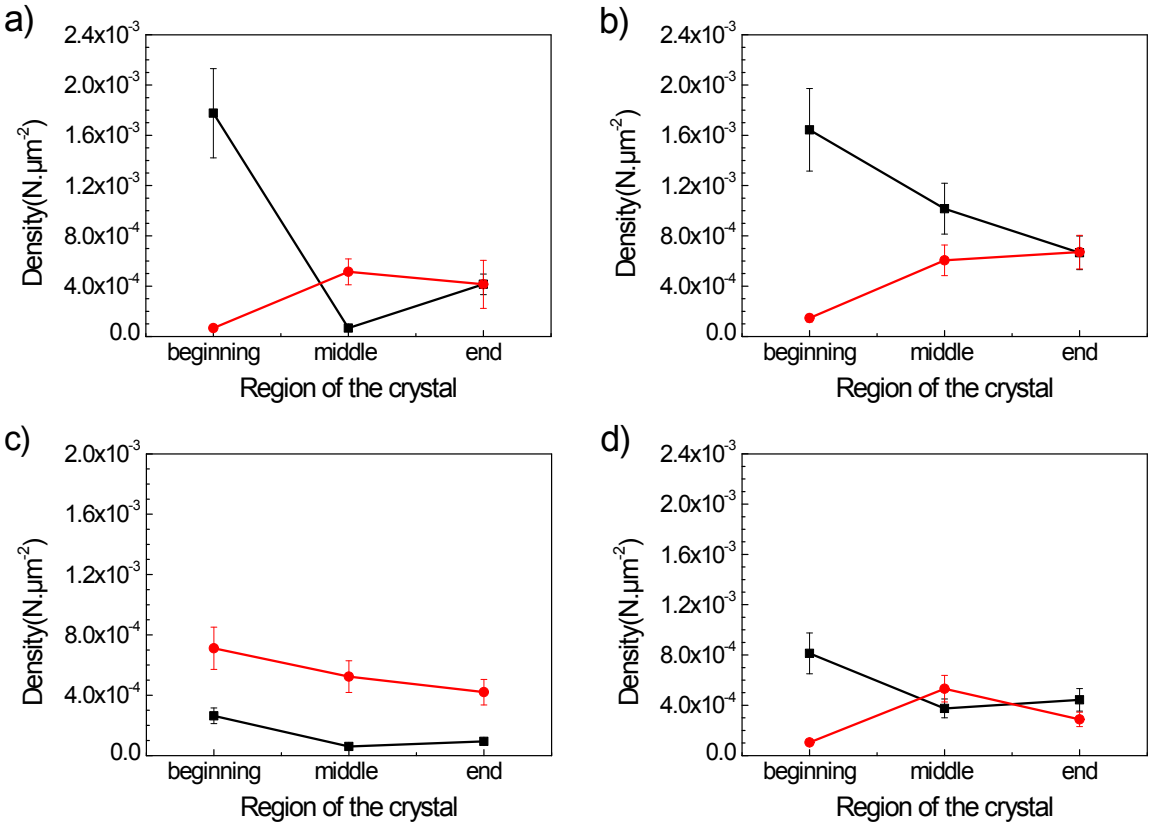

Fig.S7. Bubbles densities variation along the rods (longitudinal), (a) a-axis; (b) m-axis; (c) c-axis and (d) the c-axis tilted of 30°. (Black squares: rods grown with the standard configuration of thermal gradient (After heater with one window (1GT)). red dots: rods grown with the configuration inducing high thermal gradient (after heater with three windows (3GT))). For all samples pulling rate was 500 µm.min^{-1}.

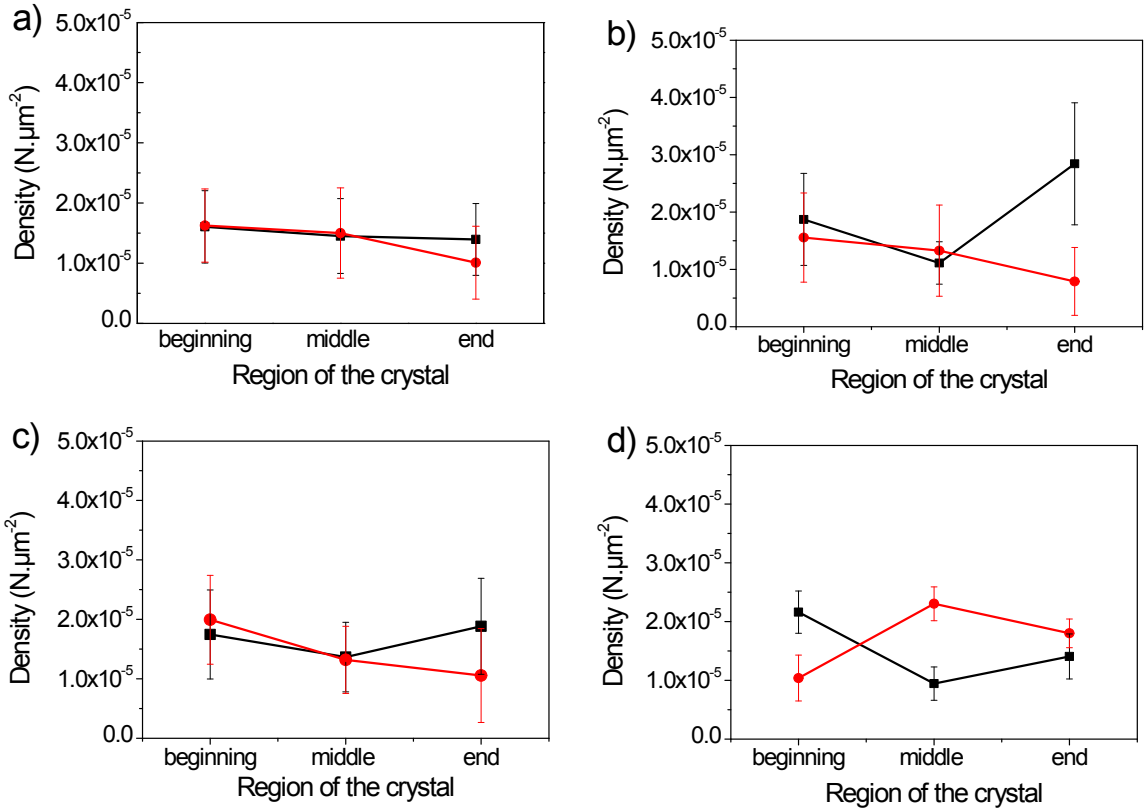

Fig.S8. Rods cross section bubbles densities measured in different parts of sapphire crystals grown along different seed orientations: (a) a-axis; (b) m-axis; (c) c-axis and (d) c tilted of 30°. The measurements on the rods grown with a standard configuration of thermal gradient around the capillary are presented by black squares. The bubbles densities measured on the rods grown with the configuration inducing high thermal gradient are presented by red dots. For all samples pulling rate was 500µm.min^{-1}.

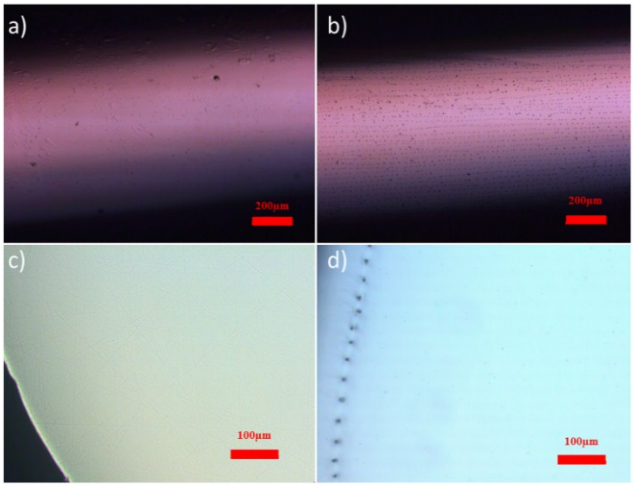

Figure 9. Bubbles density variations as a function of the pulling rates. Observation on the lateral periphery of the grown rod in (a) V = 100 µm.min^{-1}; (b) V =1200 µm.min^{-1}. Observation on the cross section of the grown rod; (c) V = 100µm.min^{-1}; d) V=1200 µm.min^{-1}

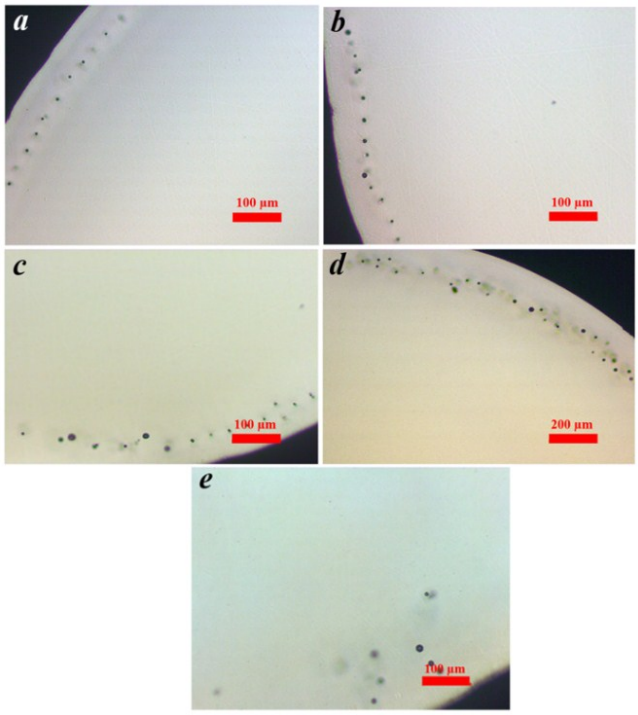

Fig.S10. Bubbles arrangement in one array at about 100µm from the periphery of the rods (a) a-axis, v=1200µm.min^{-1}, 1GT=40°C/mm, (b) a-axis, v=1200µm.min^{-1} , GT=55°C/mm, (c) m-axis, v=1200 µm.min^{-1} , GT=40°C/mm, (d) c+30°-axis, v=1200µm.min^{-1}, GT=55°C/mm, (e) c-axis, v= 500µm.min^{-1}, 1GT=40°C/mm.

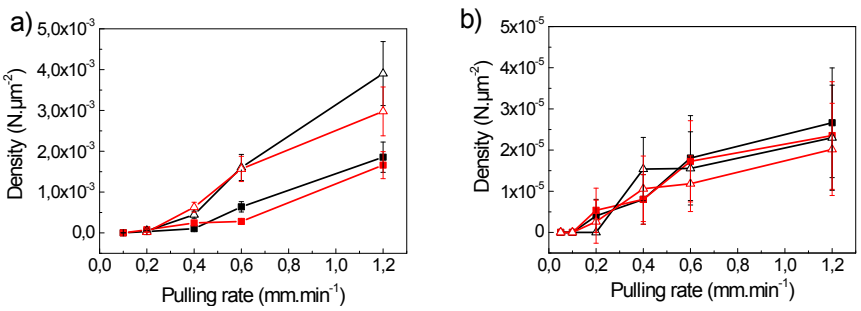

Fig.S11. (a) Bubbles densities evolution on the barrel, (b) bubbles densities evolution on the cross section. (Squares = a-axis; triangles = m-axis; red = standard thermal gradient; black = high thermal gradient).

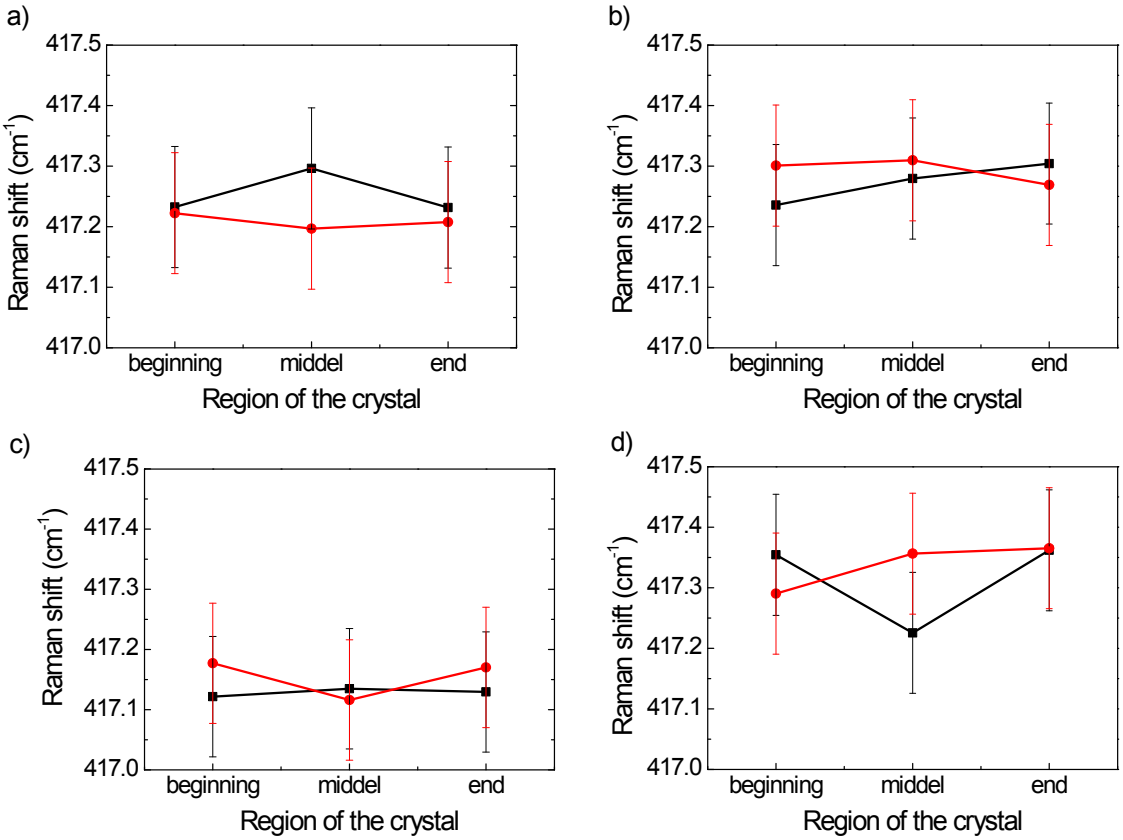

Fig.S12. Peak positions of the A_{1g} mode around 417 cm^{-1} as a function of the position in the rod. (a) a-axis; (b) m-axis; (c) c-axis and (d) the c tilted of 30°. In black, measurements realized on a rods grown with the standard configuration of thermal gradient (1GT). In red, measurements realized on a rods grown with the configuration inducing high thermal gradient (3GT).

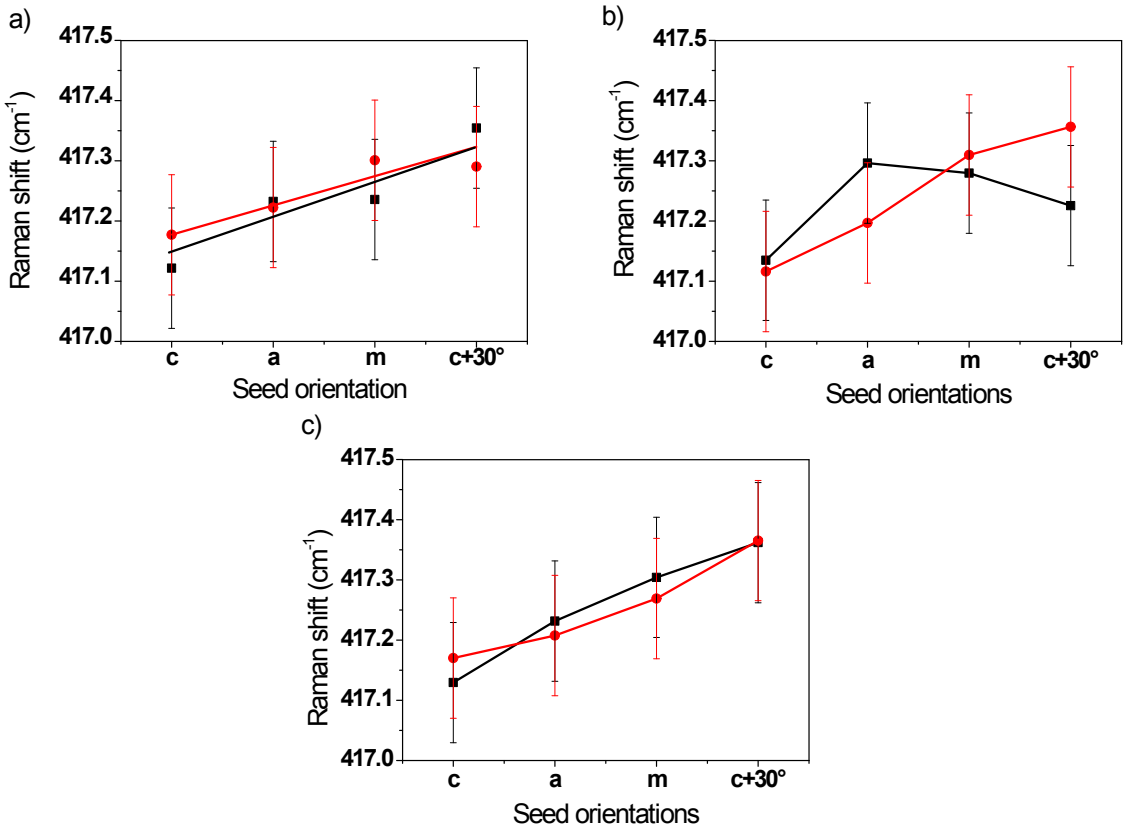

Fig.S13. Peak positions of the A_{1g} mode around 417 cm^{-1} in function of the seed orientations, (a) in the beginning; (b) in the middle, and (c) in the end of the rod. In black, measurements realized on a rods grown with the standard configuration of thermal gradient (1GT). In red, measurements realized on a rods grown with the configuration inducing high thermal gradient (3GT).

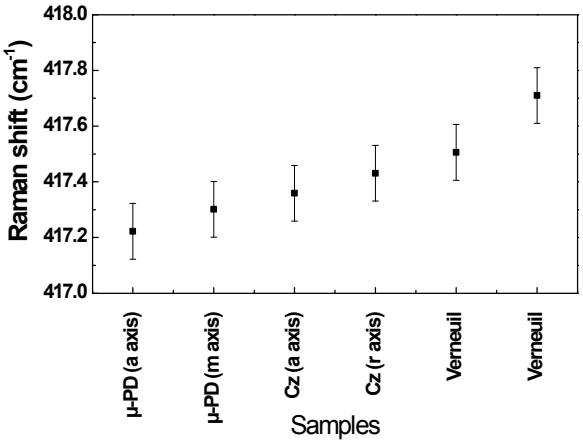

Figure 14. Peak positions of the A1g mode around 417 cm^{-1} in function of the grown techniques and seed orientations.

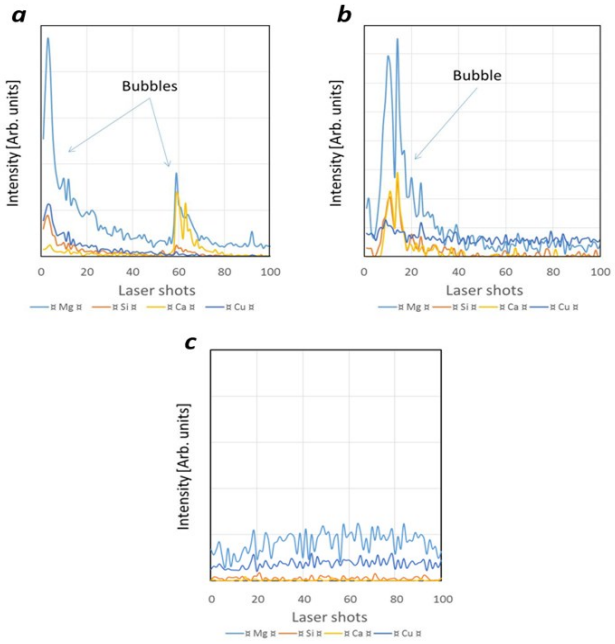

Figure 15. LIBS measurements performed on (a) a bubble just below the surface and a second one deeper, in (b) a single bubble below the surface and in (c) region of sapphire rod without bubbles. Spectra intensities of different impurities are present in function of the laser shots number.

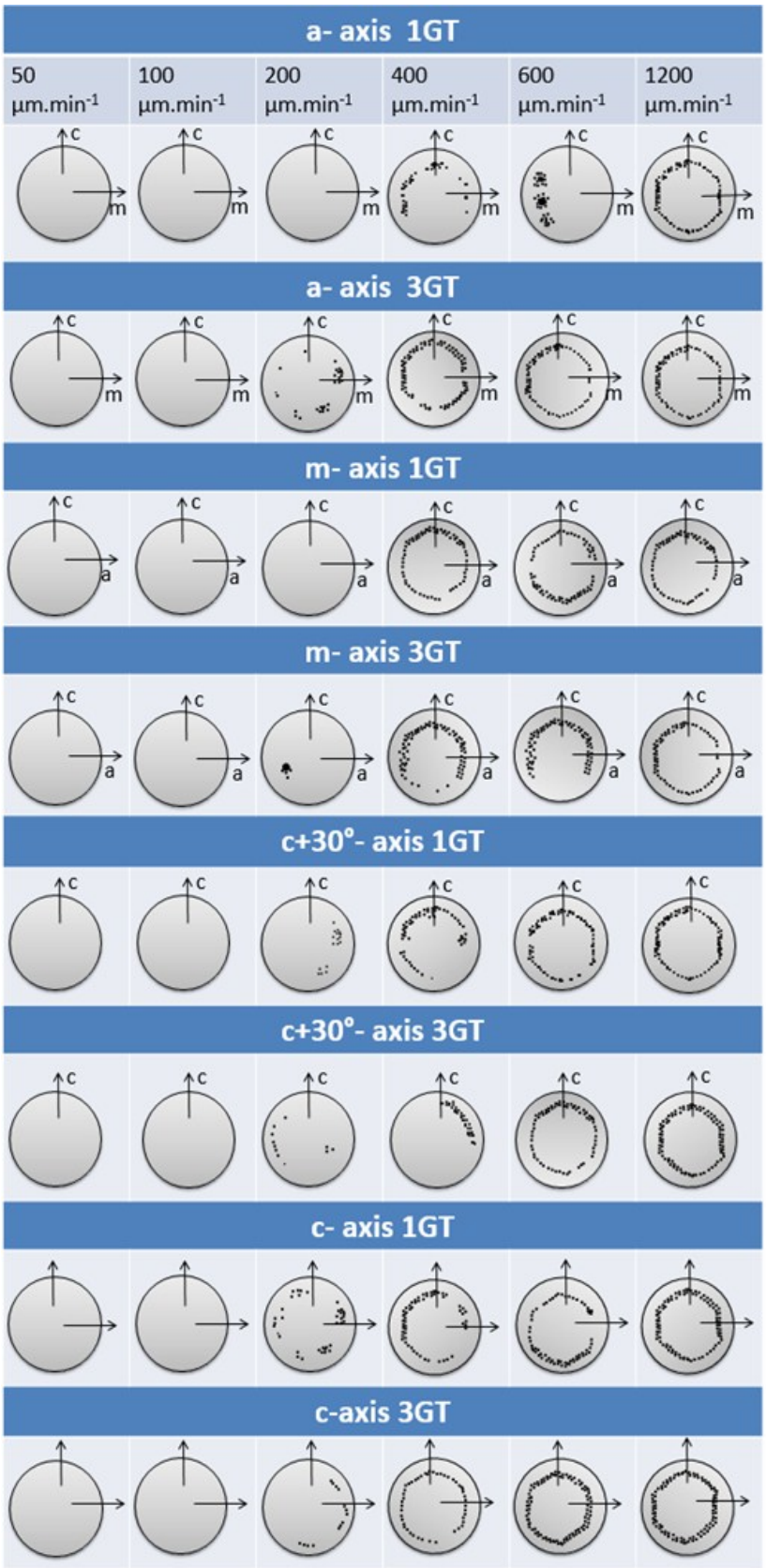

Fig.S16. Schematic illustration of bubbles distribution as a function of pulling rate, seed orientation and thermal gradient (1GT: standard thermal configuration, 3GT: high thermal gradient configuration). The crystallographic orientations are indicated by arrows.